

# Spectral density of the Hubbard-model by the continued fraction method

R. Hayn,<sup>1</sup> P. Lombardo,<sup>1</sup> and K. Matho<sup>2</sup>

<sup>1</sup>*Laboratoire Matériaux et Microélectronique de Provence,  
Faculté St. Jérôme, Case 142, F-13397 Marseille Cedex 20, France*

<sup>2</sup>*Centre de Recherches sur les Très Basses Températures,  
Laboratoire associé à l'Université Joseph Fourier,  
CNRS, BP 166, F-38042 Grenoble Cedex 9, France*

(Dated: August 30, 2018)

We present the continued fraction method (CFM) as a new microscopic approximation to the spectral density of the Hubbard model in the correlated metal phase away from half filling. The quantity expanded as a continued fraction is the single particle Green function. Leading spectral moments are taken into account through a set of real expansion coefficients, as known from the projection technique. The new aspect is to add further stages to the continued fraction, with complex coefficients, thus defining a terminator function. This enables us to treat the entire spectral range of the Green function on equal footing and determine the energy scale of the Fermi liquid quasiparticles by minimizing the total energy. The solution is free of phenomenological parameters and remains well defined in the strong coupling limit, near the doping controlled metal-insulator transition. Our results for the density of states agree reasonably with several variants of the dynamical mean field theory. The CFM requires minimal numerical effort and can be generalized in several ways that are interesting for applications to real materials.

PACS numbers: 71.10.Fd, 75.20.Hr

## I. INTRODUCTION

The Hubbard Hamiltonian<sup>1</sup> is certainly the most important model in the field of strongly correlated electrons. The spectral function for the addition or removal of a single electron near half filling serves as a paradigm for the excitation spectrum of highly correlated electrons in the vicinity of a Mott transition. It was a great success of the dynamical mean field theory<sup>2</sup> (DMFT) to connect the high- and low-energy parts of the spectral function in a non-perturbative solution for arbitrary interaction strength. Especially, it was confirmed that the coherent low energy excitations in the metallic phase follow the same dynamics as the Kondo resonance in the Anderson impurity-model, the other generic Hamiltonian for correlated electrons that is much better understood.<sup>3</sup>

The analog to the Kondo resonance in the impurity model is a quasiparticle (QP) band in the lattice model. Both straddle the chemical potential  $\mu$ , i.e. the lowest excitations are gapless. In the strong coupling limit, the spectral weight  $Z$  of the QP band is small, relative to two sidebands, further removed from  $\mu$ . These sidebands are called the Hubbard bands because they are roughly reminiscent of the Hubbard-I solution.<sup>1</sup> In the doping controlled regime,<sup>4</sup> one sideband always overlaps with the QPs, the other represents true high energy excitations across the correlation gap.

Hubbard-I is an approximation close to the atomic limit, but nevertheless taking exact spectral moments of the itinerant propagator up to the second order into account. It can be considered the ancestor of the projection technique<sup>5</sup> which systematically incorporates spectral moments of higher order. These approximations have severe deficiencies in the low energy sector, unless the mo-

ment series can be effectively summed up. In particular, generating a third pole in the spectral function from the high energy side alone leads to uncontrolled results.

When the density of states (DOS), as obtained within DMFT, is resolved with respect to the wavenumber  $k$ , more details about the coexistence of this Kondo resonance with atomic like features in a lattice system are revealed. The lowest excitations are true Fermi liquid (FL) QP's: (i) The finite DOS at  $\epsilon = \mu$  corresponds to longlived excitations. (ii) These are located in  $k$ -space on a Fermi surface (FS) that satisfies Luttinger's theorem.<sup>6</sup> (iii) As function of the distance  $k - k_F$  from the FS, the excitation energy has a linear, strongly reduced dispersion. (iv) The damping is quadratic in  $k - k_F$  but strongly enhanced, meaning that the linear and quadratic term are of the same order at a very small energy scale, the coherence energy  $\Delta^*$ . The two atomic like excitations turn out to be strongly damped, even when  $k$  is on the FS. Their peaks disperse with  $k$  but spectral tails spread over the entire bandwidth.

The DMFT thus unites atomic and itinerant features in a non perturbative approximation. It is exact only in dimension  $d = \infty$ . As a generic scenario, it is expected to hold down to  $d = 2$ , albeit with the caveat that the DMFT suppresses additional structure due to bosonic couplings. Earlier approximations at finite  $d$  already yielded QP's<sup>7,8</sup> and established a connection to the Kondo effect.<sup>3</sup> The high prestige of the DMFT is due to its ability to produce a selfconsistent, numerically manageable approximation to the spectral function for all energies, in particular to the parameter  $Z$  that governs the low energy sector. This has opened a path to realistic modeling of correlated materials beyond the Hubbard model in such methods as LDA+DMFT.<sup>9</sup>

It is nevertheless desirable for several reasons to pursue alternative methods in parallel. Firstly, a  $k$ -independent selfenergy, which is the proper result at  $d = \infty$ , does not allow to explain phenomena that depend on the different symmetry directions in the Brillouin zone, especially in high temperature superconductors and other low dimensional systems. Cluster extensions of the DMFT go in the direction of lifting this restriction,<sup>10</sup> but these generalizations are numerically even more demanding than the DMFT itself. The precise solution of a manybody Kondo problem is required at each iteration step towards selfconsistency. In practice, when designing the "impurity solver", a trade-off exists between improving the low energy, low temperature solution and exactly satisfying global sumrules. Such numerical problems are presently a bottleneck for extensions of the DMFT to larger clusters or to LDA+DMFT with charge transfer into ligand bands. A variational aspect was recently found, which may allow to circumvent some of the numerical problems.<sup>11</sup>

In this paper, we present a continued fraction method (CFM) and implement it for the doping controlled metallic regime near the Mott transition. Similar to other recent attempts,<sup>12,13,14,15,16</sup> we start from the projection technique, applied to the  $k$ -resolved single particle Green function (GF). The notations are introduced in section II. In section III, the connections between the moment- and continued fraction- (CF) expansion as well as the Padé approximant (PA) are established. In the PA, qualitatively important features of the macroscopic system, such as damping, are missing. They can only be captured by resummation of the CF to infinite order. The concept of a terminator function (TF), by which an approximate resummation is achieved, is common to many methods based on the CF. As a general scheme, we define our CFM by allowing only such TF's that preserve the structure of a truncated CF, however with complex coefficients. Useful recursion relations, that are properties of PAs, can thus be carried over and the solution for the GF can be constrained by high as well as low energy sumrules.

Previous solutions obtained with this ansatz<sup>13</sup> were partly phenomenological, because the strong coupling renormalization  $Z$  needed to be inferred from a separate Gutzwiller approximation, or else was left open for fitting to experiments.<sup>17,18</sup> A closed solution is now achieved by minimizing the total energy in the presence of sumrules, for which the necessary selfconsistency loops are introduced. The selfconsistent  $Z$  falls below the Gutzwiller value and has a doping dependence close to that for the exact Kondo scale.<sup>19</sup> This is now a true microscopic approximation, depending only on the parameters in the Hamiltonian.

In sections IV, V and VI we have investigated the TF's that correspond to adding one or two stages with complex coefficients to the CF. We show how the FS singularity, the enclosed Luttinger volume in  $k$ -space and the FL damping can be modeled rigorously. We assess the qual-

ity of our approximations by comparing the DOS with the DMFT result for two variants of the impurity solver, namely the numerical renormalization group (NRG)<sup>20</sup> and the non-crossing approximation (NCA).<sup>21</sup>

The success of the CFM with respect to the Hubbard model allows to draw some optimistic conclusions about possible generalizations towards more realistic models, describing correlation effects in a multiband electronic environment. This will be outlined as part of the conclusions.

## II. HAMILTONIAN, GREEN FUNCTION AND GENERALITIES ABOUT CONTINUED FRACTIONS

The Hubbard model for a grand canonical ensemble of electrons on a lattice of  $N$  sites ( $N \rightarrow \infty$ ) is written in the usual notations

$$\hat{H} = H - \mu \hat{N} = \sum_{k,\sigma} (E_k - \mu) c_{k\sigma}^\dagger c_{k\sigma} + U \sum_i n_{i\uparrow} n_{i\downarrow}. \quad (1)$$

The kinetic energy consists of itinerant Bloch states with energies  $E_k$  and wavenumber  $k$ , running through one Brillouin zone. The bandwidth is  $2D$  and, when not specified otherwise,  $D$  is used as unit of both energy and frequency ( $\hbar = 1$ ). We formulate the method for an arbitrary density of Bloch states. Numerical examples later on will be calculated for a semi-elliptic density.

The chemical potential  $\mu$  is selfconsistently determined to satisfy the condition

$$n = \langle \hat{N} \rangle / N = 2m = \sum_{\sigma} \overline{\langle c_{k\sigma}^\dagger c_{k\sigma} \rangle}, \quad (2)$$

where the filling factor  $n$  ( $0 \leq n \leq 2$ ) is part of the input. The chemical potential for the  $U = 0$  limit is designated as  $\mu_0$ . For  $U \neq 0$ , the right hand side is calculated with our method. The overline and the bracket signify Brillouin zone average and ensemble average, respectively. The filling factor per spin direction in the spin degenerate phase is  $m = n/2$ .

We approximate the advanced single particle GF

$$G(k, \omega) = i \int_{-\infty}^0 e^{i\omega t} \langle [c_{k\sigma}(t), c_{k\sigma}^\dagger(0)] \rangle, \quad (3)$$

from which the momentum distribution  $\langle c_{k\sigma}^\dagger c_{k\sigma} \rangle$  and other observables are calculated. The spin index is dropped in the unpolarized phase. The time dependent fermionic destruction operator  $c_{k\sigma}(t)$  is in the Heisenberg representation with  $\hat{H}$  and the square bracket is the anticommutator. The complex frequency  $\omega$  has  $\mu$  as origin. Asymptotically, for large  $\omega$ , we have  $G(k, \omega) \simeq 1/\omega$ . The coefficient 1 reflects the moment  $M_0 = 1$  or spectral norm, as required by the Pauli principle. For this relation between the leading coefficient and the norm to remain

valid in an approximation, it is necessary and sufficient to conserve the Herglotz property. In the case of the advanced GF, it means that the relation  $\text{Im}G(k, \omega) > 0$  must be obeyed throughout the entire halfplane  $\text{Im}\omega < 0$ . The physical meaning of the Herglotz property is causality and it automatically entails the existence of Kramers-Kronig relations between the real and imaginary parts. A great advantage of our method is the possibility to make straightforward evaluations along the real axis. Since this limit has to be approached from within the domain of analyticity, the notation  $\omega = \epsilon - i0^+$  with real energy  $\epsilon = E - \mu$  is introduced. The  $k$ -resolved spectral function is

$$A(k, \epsilon) = \frac{1}{\pi} \text{Im}G(k, \epsilon - i0^+). \quad (4)$$

At  $U = 0$  it has a single sharp peak at the excitation energy

$$\eta_k = E_k - \mu_0 \propto (k - k_F), \quad (5)$$

which also serves to measure distance in  $k$ -space, at least in the vicinity of the FS.

The CF expansion, on which our method is based in a crucial way, has already a long tradition in solid state physics, in the one electron problem with disorder<sup>23</sup> as well as in the many electron problem.<sup>24</sup> The CF is generated by various procedures like tridiagonalization, recursion- or Lanczos-methods. The Hubbard-I GF is the simplest example of a CF that has been truncated at low order. The exact GF for the Hubbard model on finite clusters is a CF which naturally ends at very high order. The CF for the infinite system does not end. Properties of the thermodynamic limit, such as damping due to electron-electron scattering, emerge only after resummation of the CF. Approximate resummation is achieved by the TF, an analytic function which also has the Herglotz property.

A well chosen TF is thus expected to bring two improvements to the approximation for the GF in dimensions  $d \geq 2$ : (i) From a set of discrete, more or less intense and more or less densely spaced Dirac peaks emerges the final shape of the continuous spectral density (see Ref. 25 for tight-binding like models and Ref. 26 for strongly correlated electrons). (ii) A Fermi surface (FS) discontinuity emerges in the momentum distribution  $\langle c_{k\sigma}^\dagger c_{k\sigma} \rangle$  at temperatures below the strong coupling energy scale  $\Delta^*$ . The FL discontinuity and the correct FS volume will be incorporated in our ansatz. This means, we take the Luttinger theorem for granted and use it as a principle, even for strong coupling where there is no rigorous proof. The energy  $\Delta^*$  then comes out as part of the selfconsistent solution.

### III. HIGH-ENERGY PART

The first moment or center of gravity of  $G(k, \omega)$  is

$$\omega_1 = E_k + mU - \mu. \quad (6)$$

It disperses like the unrenormalized Bloch energy  $E_k$ . In models with a more general interaction, a  $k$ -dependent Hartree-Fock shift is also present which, for onsite repulsion, reduces to a constant Hartree shift  $mU$ . The selfconsistent  $\mu$  is the only unknown.

The high energy expansion about the center of gravity is

$$G(k, \omega) = \frac{1}{\omega - \omega_1} + \frac{M_2}{(\omega - \omega_1)^3} + \frac{M_3}{(\omega - \omega_1)^4} + \dots \quad (7)$$

Its coefficients

$$M_\lambda = \int_{-\infty}^{\infty} d\epsilon \cdot (\epsilon - \omega_1)^\lambda A(k, \epsilon); \quad \lambda = 2, 3, \dots \quad (8)$$

are called the central moments ( $M_1 = 0$ , by definition). They can be related to correlation functions which occur in the short time, or Liouville expansion of the operator  $c_{k\sigma}(t)$  and are evaluated in the limit  $t = 0$ .

It is remarkable that the variance  $s_2$  of  $A(k, \epsilon)$ , defined by the second central moment

$$M_2 = s_2^2 = m(1 - m)U^2 \quad (9)$$

is  $k$ -independent in any dimension  $d$ , not only  $d = \infty$ . All the terms in the high energy expansion are sensitive to the low energy sector, be it only via the selfconsistent  $\mu$ .

We now turn to the CF expansion which is closely related to the moment expansion. Formally, it is initiated by using  $\omega_1$  and  $s_2$  to write the GF as

$$G(k, \omega)^{-1} = \omega - \omega_1 - s_2^2 G_1(\omega). \quad (10)$$

In this identity,  $G_1(\omega)$  is again a Herglotz function with asymptotics  $G_1(\omega) \simeq 1/\omega$ . Iterations, pushing the CF further down step by step, require knowledge of the center of gravity  $\omega_{2l-1}$  and the variance  $s_{2l}$  of  $G_{l-1}(\omega)$ , to write

$$G_{l-1}(\omega)^{-1} = \omega - \omega_{2l-1} - s_{2l}^2 G_l(\omega), \quad l = 2, 3, \dots \quad (11)$$

The two new expansion coefficients depend only on the central moments  $M_\lambda$  up to the order  $\lambda = 2l - 1$  and  $\lambda = 2l$  of their respective index.

By truncating the CF, i.e. by setting  $G_l(\omega) \equiv 0$ , an approximation to the GF is obtained that has  $l - 1$  zeros and  $l$  poles on the real axis. This is defined<sup>27</sup> as the PA  $\langle l - 1 | l \rangle$ . It represents the optimal use one can make of a set of known spectral moments up to  $M_{2l-1}$ . The present task, constructing the GF, is rendered essentially more difficult, because the moments themselves are not yet known. A solution based on a PA can be made selfconsistent but the moments turn out to be numerically quite inexact. This fact is often ignored when it is claimed that a certain high energy approximation obeys a set of "exact" sumrules.

We now discuss some well known results concerning approximations at the second stage of the CF. As a still

exact representation of the GF we have

$$G(k, \omega) = \frac{1}{\omega - \omega_1 - \frac{s_2^2}{\omega - \omega_3 - s_4^2 G_2(\omega)}}. \quad (12)$$

The relations between the first few terms are:

$$\begin{aligned} s_2^2 &= M_2 \\ \omega_3 &= \omega_1 + M_3/M_2 \\ s_4^2 &= M_4/M_2 - M_2 - (M_3/M_2)^2. \end{aligned} \quad (13)$$

Besides the variance, quantities used to further characterize the internal shape of a spectrum are the skewness  $\gamma = M_3/M_2^{3/2}$  and the kurtosis  $\kappa = M_4/M_2^2 - 3$ . In terms of these, we have  $\omega_3 = \omega_1 + \gamma s_2$  and  $s_4^2 = s_2^2(\kappa + 2 - \gamma^2)$ . From the third moment one finds the coefficient

$$\omega_3 = (1 - m)U + B_3 - \mu. \quad (14)$$

This CF coefficient is the first quantity in the expansion with a non trivial  $k$ -dependence. The full correlation function appearing in the third moment was first derived in Ref. 28 and determined selfconsistently for a short linear chain in Ref. 29. The shift in the spectral skewness, caused by  $B_3$ , regulates the dynamical weight transfer between the Hubbard peaks at finite  $U$ .<sup>30</sup> One can decompose

$$B_3 = W_0 + W_3(k) \quad (15)$$

in such a way that the term  $W_3(k)$  vanishes in high dimensions. For making contact with the DMFT we will presently neglect it and adopt the expression<sup>28</sup>

$$B_3 = \frac{(2m - 1)}{2m(1 - m)} \langle \hat{T} \rangle, \quad (16)$$

by which it is linked selfconsistently to the expectation value of the kinetic energy  $\langle \hat{T} \rangle$ .

Concerning the behavior of the fourth moment, not even the correlation functions involved in its selfconsistency loop have as yet been evaluated. Again, the actual numerical value of  $s_4^2$  is also expected to be sensitive to the low energy sector and, in low dimensional systems,  $k$ -dependent.

Given this situation, approximations on the level of Eq. (12) are at present inevitable. Straightforward truncation,  $G_2(\omega) = 0$ , leads to the PA  $\langle 1|2 \rangle$ . This solution with two Dirac peaks goes beyond Hubbard-I, because the dynamical weight transfer is taken into account. The first example of an approximate resummation of the CF is the alloy analogy, developed in the paper called Hubbard-III.<sup>31</sup> Following Hubbard's notation, we approximate  $s_4^2 G_2(\omega)$  by a  $k$ -independent TF  $\Omega_H(\omega)$ , which has to be a Herglotz function.

The alloy analogy satisfies at least the task (i) of a TF, namely to generate finite damping. Far away from  $\mu$ , where the excitations are incoherent, it actually represents a physically correct picture. We therefore keep the

result  $\Omega_H(\omega) \rightarrow iD$  for large  $\omega$  from Hubbard-III. The physical reason, why the damping is of the order of the bare bandwidth  $D$  is that the mean free path is as short as one lattice constant. In practice, we incorporate the high energy damping in an effective  $\omega_3$

$$\bar{\omega}_3 = \omega_3 + iD \quad (17)$$

and henceforth deal with a terminator that decays as  $1/\omega$ . This way, we conserve the sumrules, encapsulated in the central moments  $M_0$  to  $M_3$ . Since Hubbard-III is unrealistic at low energies, we do not pursue it any further. Nevertheless, it should be noted that Hubbard-III generates a branchcut in  $\Omega_H(\omega)$ , causing the imaginary part to drop back to zero and a correlation gap with sharp edges to appear, at least in the zero temperature limit. This property of Hubbard-III is also not expected to survive in improved approximations for the metallic phase. We will address the consequences that the absence of a branchcut has for the shape of the DOS, both in the CFM and in the DMFT.

To sum up, our approximation to the GF is formally similar to Hubbard-III,

$$G(k, \omega) = \frac{1}{\omega - \omega_1 - \frac{s_2^2}{\omega - \bar{\omega}_3 - \Omega(\omega)}}, \quad (18)$$

but with a TF,  $\Omega_H(\omega) = \Omega(\omega) + iD$ , that retains the strong damping of the alloy analogy only at high energy. Two successive implementations of the TF with appropriate FL properties at low energy, are the subject of the following sections.

#### IV. LOW-ENERGY PART

A FS discontinuity is strictly realized only in the zero temperature limit and in a system with no residual disorder. Since  $T = 0$  solutions are hardest to obtain with DMFT and, on the contrary, easily implemented with our method, we concentrate in the following on this limit. We write the standard microscopic definition of a selfenergy as a complex correction to the bare excitation  $\eta_k$ :

$$G(k, \omega)^{-1} = \omega - \eta_k - \Sigma(k, \omega) \quad (19)$$

and compare with the inverse of Eq. (18). The high energy limit  $\Sigma(k, \infty)$  is the difference between two dispersive quantities. In the present case, Eqs. (5) and (6) have identical dispersion and

$$p_1 = \eta_k - \omega_1 = \mu - \mu_0 - mU \quad (20)$$

is, in fact, constant. Within the other approximations, discussed in the preceding section, we then obtain the  $k$ -independent selfenergy

$$\Sigma(\omega) = -p_1 + \frac{s_2^2}{\omega - \bar{\omega}_3 - \Omega(\omega)}. \quad (21)$$

In this case, as in the DMFT, the FS has the exact shape of the uncorrelated system. It is given by all  $k$ -points where  $\eta_k = 0$  in Eq. (5). The QP peak of weight  $Z$  at the Fermi level and the step of amplitude  $Z$  in the momentum distribution are fixed by the conditions

$$\Sigma(0) = 0 \quad (22)$$

and

$$\frac{d\Sigma}{d\omega}(0) = \alpha = 1 - 1/Z < 0. \quad (23)$$

At finite  $T$  or in the presence of a residual diffusive mean free path,  $\text{Im}\Sigma(0)$  remains finite.

Guided by the insight that the strong coupling peak is distinct from the Hubbard peaks, we can formulate a minimal ansatz for the TF<sup>13</sup> as

$$\Omega(\omega) = \frac{(\bar{s}_4)^2}{\omega - \bar{\omega}_5}. \quad (24)$$

Adding a new stage to the CF is the proper way to "add" a pole to the GF. When this TF is inserted in Eq. (18), it generates a GF with three complex zeros in the denominator and two zeros in the nominator, i.e. the same structure as the PA  $\langle 2|3 \rangle$ . The connection of the parameters  $\bar{s}_4^2$  and  $\bar{\omega}_5$  to central moments  $M_4$  and  $M_5$  is lost. In fact, the very existence of moments beyond  $M_3$  has been sacrificed by admitting  $\bar{\omega}_3$ ,  $\bar{s}_4$ , and  $\bar{\omega}_5$  as complex quantities. They now have to be determined from conditions (22) and (23).

For the Herglotz property one finds

$$(\text{Im}\bar{s}_4)^2 / \text{Im}\bar{\omega}_5 \leq \text{Im}\bar{\omega}_3 = D \quad (25)$$

as a necessary and sufficient condition. This causes all three poles to lie in the upper half-plane. Further, it guarantees a normalized, positive semidefinite  $A(k, \epsilon)$ , which also implies quite intricate relations between the complex residues.

Now, the important point is the following: This simple ansatz is so heavily constrained by sumrules that it offers a selfconsistent solution of the problem, without any free parameters. It remains to substantiate this claim and then to discuss the quality of the solution.

After inserting Eq. (24) in Eq. (21), the conditions (22) and (23) can be brought into a system of two linear equations for the unknowns  $\bar{s}_4^2$  and  $\bar{\omega}_5$ . The determinant of this system is

$$\det_2 = -p_1^2 - \alpha s_2^2, \quad (26)$$

and the Herglotz property requires  $\det_2 > 0$ . This is a constraint on the QP weight  $Z$ : In stead of  $Z \leq 1$  (Pauli principle) we have  $Z < s_2^2 / (s_2^2 + p_1^2)$ . Closer inspection reveals that it means the QP cannot take more spectral weight than the peak in the PA  $\langle 1|2 \rangle$  that is nearest to  $\mu$ . Since around half filling this weight stays above 1/2, it is indeed only a weak constraint.

The solution

$$\bar{s}_4^2 = \frac{p_2^2}{\det_2}, \quad (27)$$

and

$$\bar{\omega}_5 = -\frac{p_1 p_2}{\det_2} \quad (28)$$

is expressed in terms of the complex quantity

$$p_2 = -(p_1 \bar{\omega}_3 + s_2^2). \quad (29)$$

It fulfills the Herglotz condition (25) with the equality sign. This is a consequence of our strong  $T = 0$  constraint  $\Sigma(0) = 0$ , concerning both the real and imaginary part. The selfenergy is now parametrized, up to  $Z$ , which remains free within a restrained interval and will be determined by minimizing the total energy.

We note, before closing this section, that Ref. 13 allows to define one-pole TF's for the more general case of a truncated GF that is expressed as a higher order PA. The general algorithm is given, by which the Eqs. (22) and (23) can be fulfilled.

## V. NUMERICAL PROCEDURE

The uncorrelated chemical potential as function of the filling,  $\mu_0(n)$ , depends only on the kinetic energy part and is determined once for all. The DOS per lattice site in the  $U = 0$  limit

$$\rho_0(\epsilon) = \frac{2}{\pi} \text{Im}F_0(\epsilon - i0^+) \quad (30)$$

is obtained from the onsite GF

$$F_0(\omega) = \frac{1}{N} \sum_k \frac{1}{\omega + \mu_0 - E_k}. \quad (31)$$

A factor two comes from summing over spin directions. The DOS of the correlated system

$$\rho(\epsilon) = \frac{2}{\pi} \text{Im}F(\epsilon - i0^+) \quad (32)$$

is obtained from  $F(\omega) = \overline{G(k, \omega)}$ , the on-site GF in real space, which is independent of the site index. For a  $k$ -independent selfenergy such as Eq. (21), the on-site GF's  $F(\omega)$  and  $F_0(\omega)$  are related to each other by

$$F(\omega) = F_0(\omega - \Sigma(\omega)). \quad (33)$$

The  $k$ -summations can then be carried out by using the analytic function that represents the solution for  $F_0(\omega)$  in the limit  $N \rightarrow \infty$ .

We now turn to the discussion of the selfconsistency loops. The condition for  $\mu$  is implemented at  $T = 0$  by the integral

$$\int_{-\infty}^0 d\epsilon \rho(\epsilon) = n. \quad (34)$$

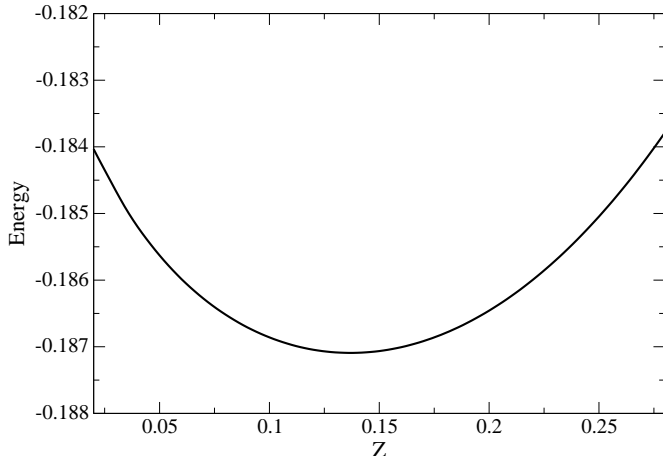


FIG. 1: Energy minimum  $E_{tot}(Z)$  for  $U = 4$ ,  $D = 1$ , and  $\mu_0 = -0.166$  corresponding to  $n = 0.79$ . The choice of  $D = 1$  means that all energies are measured in units of the halfwidth  $D$  of the uncorrelated band.

According to Eq. (16), the term  $B_3$  from the third moment requires the selfconsistent determination of the kinetic energy,  $\langle \hat{T} \rangle = 2 \int_{-\infty}^0 d\epsilon \overline{A(k, \epsilon) E_k}$ . One finds

$$\begin{aligned} \langle \hat{T} \rangle &= \frac{2}{\pi} \int_{-\infty}^0 d\epsilon \text{Im}(\tilde{\omega} F_0(\omega - \Sigma(\omega)) - 1) \quad (35) \\ \tilde{\omega} &= \epsilon - i0^+ + \mu_0 - \Sigma(\epsilon - i0^+). \end{aligned}$$

Finally, the total energy is

$$E_{tot} = \frac{1}{2} (\langle \hat{T} \rangle) + \int_{-\infty}^0 d\epsilon \epsilon \rho(\epsilon). \quad (36)$$

The integrals in (34) - (36) are carried out numerically. For the calculations in this paper we took the on-site GF

$$F_0(\omega) = \frac{2}{(\omega + \mu_0) \left( 1 + \sqrt{1 - \frac{1}{(\omega + \mu_0)^2}} \right)}. \quad (37)$$

In the context of  $d = \infty$ , it is the GF for a Bethe lattice. A halfwidth  $D = 1$  is now used as energy unit. For the Herglotz property, it is important to choose the square root with a positive real part. The model DOS belonging to this GF,

$$\rho_0(\epsilon) = \frac{4}{\pi} \sqrt{1 - (\epsilon + \mu_0)^2} \quad (38)$$

is the semi-elliptic function which was also used by Hubbard.

While searching for the selfconsistent  $\mu$  and  $\langle \hat{T} \rangle$  at a given input  $n$  and  $U$ , the renormalization  $Z$  is still kept as a parameter, only limited by the condition  $\det_2 > 0$ .

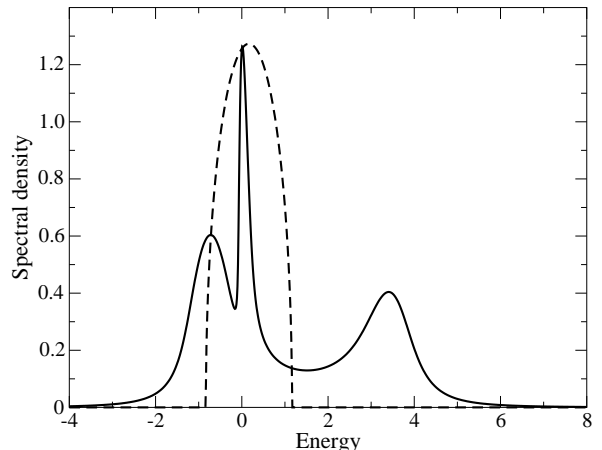


FIG. 2: Spectral density, comparison of  $\rho_0(\epsilon)$  (dashed line) and  $\rho(\epsilon)$  (full line) for the same parameters as in Fig. 1.

With these constrained solutions for the GF, we calculate the total energy  $E_{tot}$ . As shown in the example of Fig. 1,  $E_{tot}$  has a well defined minimum as a function of  $Z$ . Taking the value which minimizes  $E_{tot}$  fixes the last parameter  $Z$  and defines our solution for the GF.

The DOS obtained for the same input as in Fig. 1 is shown in Fig. 2, together with the  $U = 0$  limit. The QP band has the same intensity at the Fermi level as the uncorrelated band,  $\rho(0) = \rho_0(0)$ . This invariance signals the unitary limit for the Kondo resonance in the limit  $T = 0$ . Thus, the reduction of the QP weight does not show up in  $\rho(0)$  but in the bandwidth, which is scaled down by  $Z$ . In a lattice system, this one-to-one relationship between QP weight and bandwidth only holds when the selfenergy is local ( $k$ -independent).

On the  $k$ -resolved level, near the FS, the QP-pole in the complex plane has a parabolic trajectory parametrized by  $\eta_k$ , Eq. (5):

$$\omega^*(k) = Z\eta_k + i\Gamma_k, \quad (39)$$

with a scattering rate

$$\Gamma_k = (Z\eta_k)^2 / \Delta^*. \quad (40)$$

The halfwidth for coherent states within the QP band is

$$\Delta^* = \frac{Zs_2^2 |p_2|^2}{D((1-Z)s_2^2 - Zp_1^2)^2}. \quad (41)$$

This formula is well behaved also in the weak coupling limit, in fact for all possible metallic, unpolarized regimes of the Hubbard model. In the strongly correlated regime, the energy scale  $\Delta^*$  is smaller than  $ZD$ , so that the excitations in the wings of the QP band cease to be

coherent. Since we have modeled the ballistic limit (residual diffusive scattering rate  $\Gamma_d = 0$ ) the QP resonance in  $A(k, \epsilon)$  is a Dirac peak for  $k = k_F$  and, for  $k \neq k_F$ , it has the so called Breit-Wigner lineshape (see Hedin and Lundquist<sup>32</sup> for a generic plot). This shape is due to an interference between the QP residue and the other residues. The lineshape becomes approximately Lorentzian whenever a  $\Gamma_d > \Gamma_k$  is present.

Returning to the DOS, we note that the global shape of the valence spectrum for a hole doped Mott insulator, i.e. QP band and lower Hubbard band, is well rendered by our present approximation. The sumrules up to  $M_3$  are exactly satisfied and their interplay regulates the overall skewness and the relative weight of all three features.

The one-pole TF has the drawback of being unable to reproduce a sharp gap formation. The high level of intensity between the QP band and the upper Hubbard band shows that the dynamical spectral transfer<sup>30</sup> is not realized completely, at least for  $U/D = 4$ . The intensity at the minimum decays like  $(U/D)^{-2}$ , so that this spurious effect disappears for larger  $U$ . We shall discuss the presence of residual intensity in the gap region in more detail when we compare with our second ansatz and with the DMFT.

Two remarks to conclude this section: (i) The limit  $U = \infty$  describes spin- and charge-excitations in the subspace of singly occupied sites. It is equivalent to the  $t - J$ -model with  $J = 0$ . The one-pole TF thus allows to project out a quantitatively valid GF for the valence sector near this limit, up to terms of order  $(U/D)^{-2}$ . (ii) Ratios  $U/D \approx 4$  are relevant for the doping controlled Mott transition in real materials close to criticality. Our main motivation to pursue the CFM was to investigate whether by simply adding a second complex stage to the TF we could handle this regime in a semiquantitative way. The derivation of the two-pole TF and its application to  $U/D = 4$  are presented in the next section.

## VI. IMPROVING THE DYNAMICAL WEIGHT TRANSFER

To generalize our ansatz, we introduce algebraic expressions for  $\Omega(\omega)$ , such that Eq. (18) can be cast into the form of a truncated CF with complex coefficients. This defines the CFM, provided the Herglotz condition is satisfied. The  $k$ -resolved GF has then the structure of a generalized higher order PA. By terminating the PA  $\langle 1|2 \rangle$ , we still retain the important sumrules that govern the dynamical weight transfer. Spectral moments beyond  $M_3$  cannot be recovered, but this may not be a great sacrifice, given the difficulties known from the projection method to obtain correct values for higher moments.

What can be gained by using complex coefficients is the possibility to model constructive and destructive interference phenomena in the GF at intermediate energies. A single feature in the spectral function can be built up by the contributions of several poles, resulting in uncommon

lineshapes. An ansatz frequently employed in the phenomenological interpretation of spectra is the superposition of complex poles with real residues (superposition of Lorentzians in the spectrum). Although this allows several peaks to coalesce, it still eliminates interference. One striking example of a Fano like interference within the coherence range of halfwidth  $\Delta^*$  is the Breit-Wigner lineshape of the QP.<sup>32</sup> As discussed in the preceding section, the complex residues of the two valence poles in the GF (arising from the one-pole TF in the large  $U$  limit) are enough to obtain this lineshape.

Likewise, the dynamical weight transfer and the formation of the correlation gap can be interpreted as a destructive interference in the intermediate energy range between the Hubbard bands. When the interference is complete the function  $G_2(\omega)$  in Eq. (12) should acquire a branchcut and a gap interval with zero DOS and sharp edges should result. This may be possible only on the insulating side of the Mott transition and strictly at  $T = 0$ . When the system is metallic and the chemical potential falls in a region of high DOS, it is satisfactory to model the correlation gap by a deep minimum. We demonstrate here that this situation is captured by a two-pole TF of the form

$$\Omega(\omega) = \frac{\bar{s}_4^2}{\omega - \bar{\omega}_5 - \frac{\bar{s}_6^2}{\omega - \bar{\omega}_7}}. \quad (42)$$

The new degrees of freedom are given by  $\bar{s}_4^2$  and  $\bar{\omega}_5$ . These will be found due to some qualitative arguments, restricting the ansatz from the start. Then,  $\bar{s}_6^2$  and  $\bar{\omega}_7$  can again be eliminated by the FL conditions of Eqs. (22) and (23), using the next iteration of the algorithm in Ref. 13.

The GF now has four poles and the Herglotz condition becomes a crucially important issue. To formulate it, for arbitrary complex values of  $\bar{\omega}_3$  to  $\bar{\omega}_7$ , seems at first sight rather difficult. The GF on the FS (Eq. (19) with  $\eta_k = 0$ ) has additive coherent and incoherent contributions,

$$\frac{1}{\omega - \Sigma(\omega)} = \frac{Z}{\omega} + G_b(\omega). \quad (43)$$

The decomposition is possible, because one pole lies exactly on the real axis. This will enable us to manage the Herglotz condition for  $\Sigma(\omega)$  more easily: from Eq. (42) we obtain a background function  $G_b(\omega)$  with three poles that can be written

$$G_b(\omega) = \frac{1 - Z}{\omega - \Omega_1 - \frac{\Sigma_2^2}{\omega - \Omega_3 - \frac{\Sigma_4^2}{\omega - \Omega_5}}}. \quad (44)$$

The new coefficients are designated by capital Greek letters. Systematically, they depend on  $Z$  and, at order  $\lambda$ , on all coefficients in Eqs. (18) and (42) with index  $\lambda' \leq \lambda$ .

Explicitly, the first three are

$$\begin{aligned}\Omega_1 &= -\frac{p_1}{1-Z} \\ \Sigma_2^2 &= \frac{Z \det_2}{(1-Z)^2} \\ \Omega_3 &= \frac{1}{p_1} \left\{ \frac{\alpha p_2 s_2^2}{\det_2} + \frac{\det_2}{\alpha} \right\},\end{aligned}\quad (45)$$

in terms of the previously defined quantities, Eqs. (9), (20), (26), and (29).

The high energy damping in the background function is

$$\text{Im}\Omega_3 = \left(1 + \frac{p_1^2}{\det_2}\right) \text{Im}\bar{\omega}_3 > \text{Im}\bar{\omega}_3 = D. \quad (46)$$

Between the coherence energy  $\Delta^*$  in Eq. (40) and the background function at the Fermi edge there is the relation

$$\Delta^* \text{Im}G_b(0) = Z. \quad (47)$$

For  $\Sigma_4 = \Omega_5 = 0$ , we recover the one-pole TF and Eq. (41) for  $\Delta^*$ . Since  $\Omega_1$  and  $\Sigma_2^2$  are real, there are now only three complex quantities and the Herglotz condition can be specified exhaustively, analogous to Eq. (25):

$$(\text{Im}\Sigma_4)^2 / \text{Im}\Omega_5 \leq \text{Im}\Omega_3. \quad (48)$$

The foregoing analysis suggests that  $\Sigma_4$  and  $\Omega_5$  are more useful than  $\bar{s}_4$  and  $\bar{\omega}_5$  as control parameters. To obtain the selfenergy, one can then use Eqs. (43) and (44). For further discussion we parametrize

$$\begin{aligned}\Omega_3 &= X_3 + iY_3 \\ \Sigma_4 &= X_4 + iY_4 \\ \Omega_5 &= X_5 + iY_5.\end{aligned}\quad (49)$$

A minimal requirement for properly defining the dynamical weight transfer is vanishing  $\text{Im}\Sigma(\epsilon - i0^+)$  in one other point  $\epsilon = x_0$  on the real axis, apart from  $\epsilon = 0$ . It happens if (and only if) the equality sign applies in (48).

This leads to the condition  $Y_4^2 = Y_3 Y_5$  and to

$$x_0 = X_5 - \frac{Y_5}{Y_4} X_4 \quad (50)$$

for the position. The Herglotz property guarantees that it is in fact a minimum. The influence of this interference on the shape of the valence spectrum is weakest for  $X_5 = 0$ . For simplicity, we also need to set  $Y_5 = Y_4 = Y_3$ , where  $Y_3$  is already defined in Eq. (46). The last parameter  $X_4 = -x_0$  is then fixed by the point with lowest intensity inside the correlation gap.

Before continuing with this ansatz, it is important to realize that it cannot apply exactly at half filling. There, the metallic phase is obtained by driving  $U/D$  below the critical ratio (so called bandwidth controlled transition).<sup>4</sup> The particle-hole symmetric DOS has a quite different

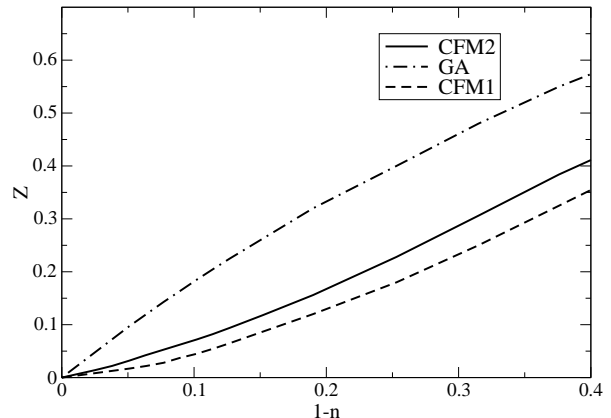


FIG. 3: Spectral weight  $Z$  of QP pole as function of electron density  $n$  for  $U = 4$ . Comparison of the Gutzwiller approximation (GA) to our result with the one- and two-pole TF's (CFM1 and CFM2).

morphology than what is shown in Fig. 2: the QP's are in the center and the correlation gap is split in two symmetric gaps of order  $U/2$ .<sup>2</sup> In our approach, it can be envisaged to use one additional complex stage to model two symmetric destructive interferences.

In the doping controlled regime, there is only one large correlation gap and we have a good qualitative argument for  $x_0$ : the strong skewness (large  $|p_1|$ ) causes the QP band and the minimum position  $x_0$  to always be on opposite sides of the center of gravity. This is well satisfied by setting

$$x_0 = \text{Re}\bar{\omega}_3. \quad (51)$$

The remaining free parameter  $Z$  is determined again by minimizing the total energy. The numerical procedure is as described before. In Fig. 3, results with the one- and two-pole TF's (CFM1 and CFM2) are compared to the Gutzwiller approximation (GA) at constant  $U$ , as function of the filling. The upper curve is the well known lower bound for the GA,  $Z = (1-n)/(1-m)$ , obtained by excluding double occupancy. By projecting out the background, the GA is known to systematically overestimate the coherent weight. The behavior that results from the CFM, i.e. : lowering of  $Z$  and upward curvature at the approach of zero doping ( $1-n \rightarrow 0$ ), is close to that of the exact Kondo scale in the Bethe ansatz solution for the Anderson impurity.<sup>19</sup>

## VII. COMPARISON WITH OTHER METHODS

With the two-pole TF, realistic results for the DOS in the doping controlled regime can be obtained, even close to the critical  $U$ . To illustrate this, we compare our



CFM with the DMFT for two different impurity solvers. The impurity solvers perform the crucial step in mapping the Hubbard lattice model onto an Anderson impurity model. The effective medium surrounding a given site is determined self-consistently, still a formidable many-body problem. The NRG,<sup>20</sup> used to solve it at the lowest temperatures and energies, requires a heavy amount of computer time. The NCA<sup>21,22</sup> is an alternative, more analytic method, less reliable for  $|\omega| \ll \Delta^*$ , but obeying high energy sumrules well. Therefore, NRG and NCA are expected to be complementary.

A comparison for the same parameters as before, i.e.  $U = 4$  and  $n = 0.79$ , is shown in Fig. 4. The NRG data are taken from Ref. 18, NCA is our own unpublished calculation, CFM1 is again the DOS from Fig. 2 and CFM2 the result with Eq. (42). All four solutions obey the  $\rho(0) = \rho_0(0)$  condition. This confirms that temperatures in the DMFT solutions are sufficiently low to warrant a comparison with our  $T = 0$  results. As manifest in the width of the QP band, the selfconsistent  $Z$  obtained for CFM2 coincides with both versions of DMFT. Since NRG is expected to determine essentially the exact low energy scale, this is a good point for both the NCA and the CFM2 results.

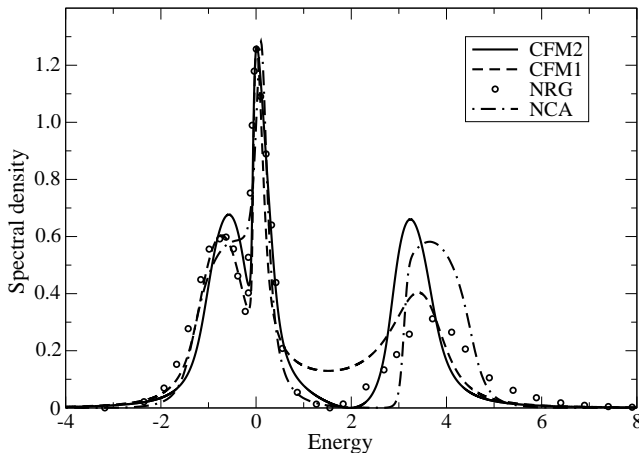


FIG. 4: Spectral density. Comparison of the continued fraction method using the one- and two pole TF's (CFM1 and CFM2) with NCA and NRG (data taken from Ref. 18).

The solutions start to differ somewhat in the gap region. Neither DMFT version shows a gap with sharp edges that would correspond to a branchcut in the self-energy. A real benchmark for low  $T$  impurity solvers in the doping controlled regime does not yet exist. From the NCA, we can confirm that some very low residual density inside the gap seems to be the generic situation.

In the ansatz for CFM2, the existence of a point with zero DOS is postulated. Determining its position according to Eq. (51) involves the selfconsistency conditions for

$\mu$  and  $B_3$ . The quantitative agreement with the DMFT in the QP band and good overall agreement in the entire valence sector is due to this built in interference. In comparing CFM1 and CFM2, one notices a feedback of the improved gap region on the QP band: The sumrules up to  $M_3$  are satisfied for both approximations, but the dynamical weight transfer is more complete within CFM2. Removing the spurious intensity inside the gap slightly raises the QP weight (Compare Fig. 3), bringing it in agreement with the NRG.

The rather large variation among the different solutions in the region of the upper Hubbard band is remarkable and still deserves more detailed investigations. At higher temperatures,  $T \geq \Delta^*$ , where Quantum Monte Carlo is available as benchmark, the NCA was found to be satisfactory.<sup>21</sup> In the present comparison, the NCA comes closer to obeying the sumrules than the NRG. As far as numerical effort is concerned, the NRG is the most demanding, followed by the NCA. The CFM2 stands up quite honorably in this comparison, especially when considering that the sumrules are rigorously incorporated, no "technical" broadening needs to be introduced and the required computer time to achieve selfconsistency is in fact negligible.

## VIII. DISCUSSION AND OUTLOOK

We present the CFM as a new method to calculate the selfenergy, as well as various  $k$ -resolved and (partially or fully)  $k$ -integrated spectral functions of the Hubbard model in the correlated metal phase. We expand the single particle Green function as a continued fraction, as far as moment sumrules are exploitable, and then use a properly chosen terminator function. In this paper, moment sumrules up to  $M_3$  are implemented and the "terminator" is a  $k$ -independent complex function with one or two poles that obeys the correct Fermi liquid properties at low energies. In this local approximation to the selfenergy, we compare our results for the density of states with the DMFT. Our method has a precision comparable to state-of-the-art impurity solvers NRG and NCA. It covers all energy scales reliably, whereas the low  $T$  impurity solvers each have their strengths and weaknesses.

With the second stage in the terminating function we are able to improve the dynamical weight transfer between the upper and lower Hubbard peak and thereby obtain very good agreement with DMFT for the QP weight  $Z$  or low energy scale. This is significant, because NRG-DMFT yields the exact result for this quantity. Unlike the time consuming DMFT calculations, the CFM uses simple, algebraic functions, for which selfconsistency conditions are rapidly found.

The CFM is generalizable in many directions. However, the possibility to circumvent heavy manybody calculations by such a simplified ansatz seems too attractive to be true. Thus, before advocating possible extensions, we need to analyze the reason for the quantitative success

of the CFM in the strong coupling limit. The Hubbard model with a local selfenergy is, admittedly, only a toy model but nevertheless an obligatory testing ground for this important issue.

The algebraic terminator functions were already introduced earlier. Their Fermi liquid properties, essential for circumventing the explicit manybody calculations, are determined by using the Luttinger sumrule as an input. Their phenomenological possibilities could be demonstrated by leaving  $Z$  as a free parameter.<sup>13,17,18</sup> The cornerstone of the CFM as a microscopic method is now the variation of the total energy to obtain  $Z$ . Given  $G(k, \omega)$ , we calculate the total energy from the exact manybody expression, actually another sumrule first found by Galitski. However, without an explicit wavefunction, we have no rigorous variational principle. In making the Gutzwiller approximation, beyond the Gutzwiller ansatz for the wavefunction, one is also abandoning the rigorous variational principle but one keeps  $Z$  as variational parameter.

The answer to the question, why our method is variational, is probably that we are using a GF, fully constrained by sumrules, that leaves no other free parameter but  $Z$ . To obtain the Kondo effect, we need degeneracy. Our model has spin degeneracy,  $N_f = 2$ , for its flavors. A clue, why including the incoherent background spectrum, instead of projecting it out, improves the outcome for  $Z$  comes from the limit of large  $N_f$ .<sup>3,19</sup> The low energy scale (Kondo temperature) in the Anderson impurity model can be obtained exactly, as function of  $n$  and  $m = n/N_f$ . Also, coherent spectral weight is of order zero in  $1/N_f$ , the leading background contribution starts at first order. Neglecting background, as for instance in the slave boson method at mean-field level, yields  $Z = (1 - n)/(1 - m)$ , as plotted for  $N_f = 2$  in Fig. 3. Compared with the Bethe ansatz, this renormalization is not enough. Now, the influence of the background is strikingly illustrated by solving for the Kondo temperature only to the first order in  $1/N_f$ .<sup>19</sup> This causes indeed a substantial decrease, bringing the result close to the exact value. The correct doping dependence displays the upward curvature, as also seen in our approximations CFM1 and CFM2. Finally, the improvement from CFM1 to CFM2 shows a delicate interplay between the dynamical weight transfer, related to the double occupancy, and the low energy scale.

If determining  $Z$  by varying the total energy is indeed a valid variational principle, it makes the CFM independent of the limit  $d = \infty$ , thus giving it high flexibility and

a large field of applications. It is straightforward and, for low dimensional systems, potentially very important to incorporate the  $k$ -dependence in the moment  $M_3$ . The term  $W_3(k)$  in Eq. (15) was already identified in the exact diagonalization of a short linear chain,<sup>29</sup> as causing a coupling of the QP to antiferromagnetic fluctuations. This can be generalized to fluctuations above other possible groundstates and the selfconsistent determination of  $W_3(k)$  thus offers a path to describing the feedback of bosonic fluctuations on the low energy sector. Up to now, the treatment of low energy effects within the projection method was based more on physical intuition, or guesswork for the more critical observer, than on an objective procedure.

The extension of the CFM to higher moments becomes possible due to its close relationship with the numerical Lanczos procedure for finite lattices. All what is missing is a proper termination of the continued fraction with a TF representing the low energy sector and the dissipation. The general algorithm for calculating the coefficients in the TF is given in Ref. 13.

As an outlook, we enumerate other possibilities that are inherent in the CFM, beyond the results of this paper. They are listed roughly according to increasing effort that will be required to implement them. (i) A more detailed exploitation of spectral functions on the  $k$ -resolved level: e.g. the interpretation of Raman, ARPES, or tunneling data requires the partial summation of  $A(k, \epsilon)$  over selected spots in the Brillouin zone, weighted by matrix elements. (ii) Hubbard lattice models with a more realistic kinetic energy part, including van Hove singularities. (iii) The generalized periodic Anderson model (PAM): lattice models with Hubbard repulsion among transition orbitals but, in addition, hybridization with ligand orbitals. (iv) Implementation of LDA+CFM. The algebraic simplicity of the CFM allows to calculate the charge transfer effects, present in model Hamiltonians of the PAM type, on an "ab-initio" level. These effects, important for many real materials, could not yet be handled successfully by LDA+DMFT. (v) Not difficult to implement, but leaving the strict framework of the CFM as an algebraic method, is the inclusion of non Fermi liquid effects on a phenomenological level.<sup>13</sup>

In conclusion, we have attempted to demonstrate by means of the Hubbard model that the CFM is a powerful method. Numerically simple, due to its algebraic structure, it is still sufficiently rigorous to deal with strongly correlated electrons in mesoscopic and macroscopic samples of condensed matter.

<sup>1</sup> J. Hubbard, Proc. Roy. Soc. A **276**, 238 (1963).

<sup>2</sup> A. Georges, G. Kotliar, W. Krauth, and M.J. Rozenberg, Rev. Mod. Phys. **68**, 13 (1996).

<sup>3</sup> A.C. Hewson, *The Kondo Problem to Heavy Fermions* (Cambridge University Press, Cambridge, 1997).

<sup>4</sup> M. Imada, A. Fujimori, and Y. Tokura, Rev. Mod. Phys.

**70**, 1039 (1998).

<sup>5</sup> H. Mori, Progr. Theor. Phys. **33**, 423 (1965); see also: P. Fulde, *Electron Correlations in Molecules and Solids* 3rd edn. (Springer-Verlag, 1995).

<sup>6</sup> J.M. Luttinger, Phys. Rev. **119**, 1153 (1960).

<sup>7</sup> D. M. Edwards and J. A. Herz, Physica B **163**, 527 (1990).

- <sup>8</sup> M.C. Gutzwiller, Phys. Rev. 137, A1726 (1965); for a review, cf. D. Vollhardt, Rev. Mod. Phys. **56**, 99 (1984).
- <sup>9</sup> K. Held et al., Psi-k Newsl. **56**, 65 (2003) (Psi-k.dl.ac.uk/newsletters/News\_56/Highlight\_56.pdf)
- <sup>10</sup> Th. Maier, M. Jarrell, Th. Pruschke, and M. Hettler, Rev. Mod. Phys. **77**, 1027 (2005).
- <sup>11</sup> M. Potthoff, M. Aichhorn, and C. Dahnken, Phys. Rev. Lett. **91**, 206402 (2003).
- <sup>12</sup> M. Potthoff, T. Herrmann, and W. Nolting, Eur. Phys. J. B **4**, 485 (1998).
- <sup>13</sup> K. Matho, J. Electron. Spectr.& Rel. Phenom. **117-118**, 13 (2001).
- <sup>14</sup> D. Villani, E. Lange, A. Avella, G. Kotliar, Phys. Rev. Lett. **85**, 804 (2000).
- <sup>15</sup> A. Avella, F. Mancini, and R. Hayn, Eur. Phys. J. B **37**, 465 (2004).
- <sup>16</sup> Y. Kakehashi and P. Fulde, Phys. Rev. Lett. **94**, 156401 (2005).
- <sup>17</sup> K. Matho, Molec. Phys. Reports **17**, 141 (1997).
- <sup>18</sup> K. Byczuk, R. Bulla, R. Claessen, and D. Vollhardt, Int. Journ. of Mod. Phys. B **16**, 3759 (2002).
- <sup>19</sup> J. W. Rasul and A. C. Hewson, J. Phys. C **17**, 3337 (1984).
- <sup>20</sup> R. Bulla, Phys. Rev. Lett. **83**, 136 (1999).
- <sup>21</sup> Th. Pruschke, D.L. Cox, and M. Jarrell, Phys. Rev. B **47**, 3553 (1993).
- <sup>22</sup> Th. Pruschke and N. Grewe, Z. Phys. B **74**, 439 (1989).
- <sup>23</sup> R. Haydock, V.Heine, M.J. Kelly, J. Phys. C: Solid State Phys. **5**, 2845 (1972).
- <sup>24</sup> E. Dagotto, Rev. Mod. Phys. **66**, 763 (1994).
- <sup>25</sup> P. Turchi, F. Ducastelle, and G. Treglia, J. Phys. C: Solid State Phys. **15**, 2891 (1982).
- <sup>26</sup> R.O. Kuzian, R. Hayn, and J. Richter, Eur. Phys. J. B **35**, 21 (2003).
- <sup>27</sup> G.A. Baker Jr., *Essentials of Padé Approximants*, Academic Press, New York (1975).
- <sup>28</sup> W. Nolting and W. Borgiel, Phys. Rev. B **39**, 6962 (1989).
- <sup>29</sup> B. Mehlig, H. Eskes, R. Hayn, and M.B.J. Meinders, Phys. Rev. B **52**, 2463 (1995).
- <sup>30</sup> M. B. J. Meinders, H. Eskes, and G. A. Sawatzky, Phys. Rev. B **48**, 3916 (1993).
- <sup>31</sup> J. Hubbard, Proc. Roy. Soc. A **277**, 237 (1963).
- <sup>32</sup> L. Hedin and S. Lundquist, *Solid State Physics*, F. Seitz, D. Turnbull, and H. Ehrenreich (eds), Vol. **23**, 1 (1969).